

---

# Event Cartography: Latent Point Process Embeddings

---

Myrl Marmarelis, Greg Ver Steeg, Aram Galstyan  
Information Sciences Institute  
University of Southern California  
myrlm@isi.edu, gregv@isi.edu, galstyan@isi.edu

## Abstract

Many important phenomena arise naturally as temporal point processes with different types of events influencing future events in complex ways. Estimation of multivariate point processes is a notorious proposition. We take inspiration from spatiotemporal point processes, where relationships depend only on relative distances in real Euclidean space, to suggest embedding arbitrary event types in a latent space. We demonstrate that we can simultaneously learn this embedding and a point process model to recover relationships among events.

## 1 Introduction & Motivation

The propagation of disease [1], news topics [2], crime patterns [3, 4], neuronal firings [5], and market trade-level activity [6, 7] are representable in their rawest forms as diachronic point processes with an underlying causal-interaction network. Understanding their intrinsic dynamics is of paramount scientific and strategic value: certain options trades may inform an observer on the fluctuating chances that other types of trades will be executed in the near future; the manner in which media coverage of some topics stokes the public’s interest in certain others’ may betray an ensuing shift in *zeitgeist*. The spread of a novel pathogen, notably COVID-19, through disjointed pockets of the globe hints to the conditions under which it ignites a pandemic, and how they might be averted [8].

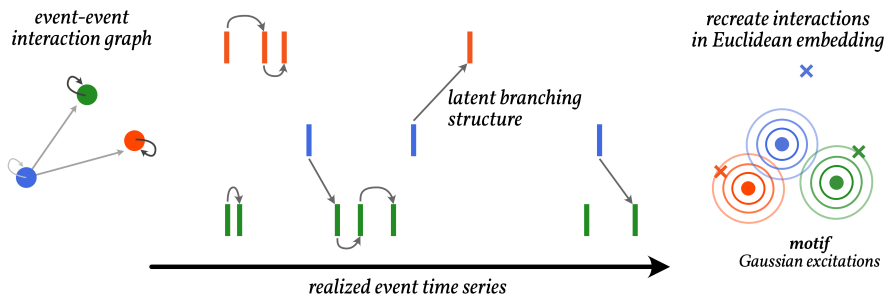


Figure 1: A stylized rendition. Instead of learning all possible interactions, we estimate a Euclidean embedding with fewer degrees of freedom and the additional benefit of interpretability.

We deem the occurrence of these events as realizations of Poisson-distributed infinitesimal random variables that make up the point process, with the intensity itself a random variate that depends on the past realizations. This is the fundamental notion driving the doubly stochastic process, first attributed to Cox [9], which stipulates the existence of a serial dependence in time. We seek to estimate an  $n$ -dimensional Hawkes-type (i.e. excitatory) model [10], assumed stationary in the interval of  $[0, T)$ .

The models deployed to capture these phenomena are notorious to estimate; moreover they yield considerable power when done effectively. The maturation of data science as a field has prompted explorations into efficient Bayesian (e.g. [11]) and scalable deep-learning (e.g. [12]) model varieties.

Spatiotemporal domains [13, 3, 14] exploit physical constraints that lead to elegant models. In essence, the influence one event bears on another is governed solely by their separation in space, and invariant to actual locations. We show that it is feasible to *learn* a spatial representation of the interacting event types by harnessing a spatiotemporal point process upon a latent embedding. The embedding and the parameters governing the process are estimated jointly.

The conceived formulation for an excitatory (marked Hawkes) point process permits the inference of an embedding directly from the likelihood function, taking inspiration from the expectation-maximization (EM) algorithm [15] employed in identifying spatiotemporal Hawkes processes [14]. Much like word embeddings extracted from text corpora and graph embeddings characterizing community structures, the latent space admits context information about each (herein discrete) event type specific to the behavior of the time series. Furthermore, we significantly reduce the dimensionality of the parameters thanks to our structural imposition of a hypothetical Euclidean space. The outcome is a succinct and interpretable parametrization for the  $(n \times n)$  allowable interactions between each possible pair (dyad) of event types. See the illustration in Figure 1 for a schematic.

To our knowledge, we are the first to propose *a vector embedding scheme driven purely by an underlying point process*. Our framework paves the way for generalization, and extension to more elaborate models in the future.

## 2 Method

### 2.1 Setup

Consider a record of  $N$  marked event occurrences  $(k_i, t_i) \in \mathbb{H}$ ,  $i = 1, 2, \dots, N$ , with  $k_i \in \{1, 2, \dots, n\}$  and  $t \in [0, T)$ . We must infer *two* sets of points  $x_k \in X$  and  $y_k \in Y$ , what we term the reception and influence embeddings respectively. Induced by a mapping  $k \mapsto (x, y)$ ,  $X$  and  $Y$  constitute the discrete  $\mathbb{R}^m$ -embedding of a latent manifold wherein the influence some event type  $l$  exerts on  $k$  is characterized by  $\|y_l - x_k\|$ . There must be distinct embeddings for receiving versus influencing because it is not always sufficient to constrain our model to symmetrically bidirectional interactions.

The multivariate intensity function  $\lambda(k, t)$ , conditional on the events in  $[0, t)$ , dictates the instantaneous Poisson frequency; a particular interval  $[t, t + dt)$  would expect to witness  $\lambda(k, t)dt$  instances of event type  $k$ . We decompose this intensity [16] into self- and cross-excitations and a background rate intrinsic to the event type.

$$\lambda(k, t) = \sum_{i=1}^N h(k, k_i, t - t_i) + \mu(k). \quad (1)$$

Each response is the result of a dyadic interaction between an event  $(k_i, t_i)$  in the past and the potential occurrence of event type  $k$  at the present time  $t$ . We chose the following parametric families for the causal kernel bank:

$$g_r(x, y) = (2\pi\beta_r^2)^{-\frac{1}{m}} \exp\left\{-\frac{\|x - y\|^2}{2\beta_r^2}\right\}, \quad (2) \quad f_r(\tau) = \delta_r e^{-\delta_r \tau}. \quad (3)$$

Eqs. 2 & 3 form the spatial and temporal basis of  $r = 1, 2, \dots, R$  kernels comprising the response function, fully expanded in Eq. 4. Later on we introduce the rest of the ingredients, namely  $\xi(k)$ .

$$h(k, l, \tau) = \mathbb{1}[\tau > 0] \sum_{r=1}^R \xi(l) \gamma_r \hat{g}_r(x_k, y_l) f_r(\tau). \quad (4)$$

A generalized Poisson process yields an elegant log-likelihood function. Given the set of points  $x \in X$  induced by  $k \mapsto x(k)$  belonging to event types  $1 \leq k \leq n$ , it may be written as follows:

$$\log L = \sum_{i=1}^N \log \lambda(k_i, t_i) - \sum_{k=1}^n \int_0^T \lambda(k, t) dt. \quad (5)$$

Suppose we happened upon the expected *branching structure* [15] of the realized point process. In other words, we introduced latent variables  $[p_{ijr}] \in \mathbb{R}^{N \times N \times R}$  holding expectation estimates of  $P_{ijr} \in \{0, 1\}$ , indicating whether it was the event instance  $i$  that triggered instance  $j$ , and attributing responsibility to kernel basis  $r$ . Knowledge of the untenable true line of causation endows us with the so-called complete-data log likelihood termed  $\log L_c$  [14], an expectation of the joint log-probability density of the record and the latent variables  $[P_{ijr}]$  in terms of their probabilities  $[p_{ijr}]$ .

$$\log L_c = \sum_{j=1}^N \left( \sum_{i=1}^N \sum_{r=1}^R p_{ijr} \log \gamma_r g_r(x_{k_j}, y_{k_i}) f_r(t_j - t_i) + p_{bj} \log \mu(k_i) \right) - \sum_{k=1}^n \int_0^T \lambda(k, t) dt \quad (6)$$

Of special note in the above form is that what was previously a logarithm of summations (see Eq. 5 and 1) is replaced by a weighted sum of decoupled logarithms. The probability that the event instance was due to the background white Poisson process is  $p_{bj}$ ;  $\forall j, \sum_{i,r} p_{ijr} + p_{bj} = 1$ . Concretely, given a model  $\lambda(k, t)$ , the allegation of causality  $i \rightarrow j$  via  $r$  is the ratio of that particular contribution to the overall intensity:

$$p_{ijr} = \frac{\mathbb{1}[\tau > 0] \gamma_r g_r(x_{k_j}, y_{k_i}) f_r(t_j - t_i)}{\lambda(k_j, t_j)}. \quad (7)$$

The right-hand term in Eq. 6 simplifies vastly if one were to assume that  $\forall y \in Y \sum_{x \in X} g(x, y) = 1$ , and that  $\int_0^\infty f(\tau) d\tau = 1$ . The latter proposition is trivially satisfied; the former is not. Only through certain concessions may we gain confidence that the sum is roughly unit. First note that, by the Gaussian integral,  $\int_{\mathbb{R}^m} g(x, y) dx = 1$ . Veen & Schoenberg [13] arrived at the conclusion that if the event occurrences in this putative space are distributed uniformly in  $\mathbb{R}^m$ , then the approximation holds arbitrarily well. Sadly our embedding scheme tends to be too coarse, and we are left with a coerced discrete normalization of Eq. 2;

$$\hat{g}_r(x, y) = \left[ \sum_{x' \in X} g_r(x', y) \right]^{-1} g_r(x, y). \quad (8)$$

We still rely on the “pure” form in Eq. 2 for the sake of closed-form optimization, as detailed below; nevertheless the surgery in Eq. 8 prevents drifting towards degeneracy. The final touch is the introduction of one more kernel parameter,  $\xi(k)$ , to account for this additional restriction. The full response kernel is therefore Eq. 4. We eliminated redundancies by constraining the *exertion coefficient*  $n^{-1} \sum_{k=1}^n \xi(k) = 1$  and scaling the *basis coefficients*  $\gamma_r$  appropriately.

## 2.2 Optimization

Furnished with the causality estimates in Eq. 7 (the “Expectation” step), we may perform projected gradient ascent by setting partial derivatives of the complete-data log-likelihood with respect to each kernel parameter to zero (the “Maximization” step). Eventually the causalities are aggregated in special ways to form coefficient estimates. Omitting the domains of summation over  $i$  and  $j$ ,  $i$  to imply  $\{1, 2, \dots, N\}$  and  $\{1, 2, \dots, N\} \times \{1, 2, \dots, N\}$  respectively, the solutions unfold as so:

$$\delta_r(\alpha_\delta, \beta_\delta) = \frac{\sum_{j,i} p_{ijr} + \alpha_\delta - 1}{\sum_{i,j} p_{ijr} (t_{k_j} - t_{k_i}) + \beta_\delta} \quad (9) \quad \gamma_r = \frac{\sum_{j,i} p_{ijr}}{\sum_i \xi(k_i)} \quad (11)$$

$$\beta_r^2 = \frac{\sum_{i,j} p_{ijr} \|x_{k_j} - y_{k_i}\|^2}{m \sum_{j,i} p_{ijr}} \quad (10) \quad \xi(l) = \frac{\sum_{r=1}^R \sum_{j,i} \mathbb{1}[k_i = l] p_{ijr}}{\sum_{r=1}^R \gamma_r \sum_i \mathbb{1}[k_i = l]}, \quad (12)$$

$$\mu(k) = T^{-1} \sum_j \mathbb{1}[k_j = k] p_{bj}. \quad (13)$$

Only the decay rate of decay  $\delta_r$  necessitated a Bayesian prior for preserving focus on the interesting time horizons. Parametrization by the Gamma( $\alpha_\delta, \beta_\delta$ ) distribution admits the maximization a posteriori in Eq. 9, which trivially becomes uninformative at the assignment  $\delta_r(1, 0)$ . One is typically interested in the half-life ( $\log 2 / \delta_r$ ), the prior of which is characterized by the aptly named inverse-gamma distribution with expectation  $\frac{\beta_\delta}{\alpha_\delta - 1}$ . Preserving the mean while increasing both parameters strengthens the prior.

The influence—also known as adjacency, affinity, proximity, depending on the field’s parlance—matrix  $\Phi = [\varphi(k, l)]$  is composed of the kernels with time integrated out, i.e.

$$\varphi(k, l) = \int_0^\infty h(k, l, \tau) d\tau = \sum_{r=1}^R \xi(l) \gamma_r g_r(x_k, y_l).$$

Persuant to the above maximization step, one may also obtain

$$\varphi(k, l) = \frac{\sum_{j,i} \mathbb{1}[k_j = k, k_i = l] \sum_{r=1}^R p_{ijr}}{\sum_i \mathbb{1}[k_i = l]}. \quad (14)$$

### 2.3 Embedding in the Latent Space

**First Principles (FP).** We invoked the direct relation between the likelihood function and the embeddings. Our approach alternates between updating the reception embedding and the influence embedding, á la Gibbs sampling. Observe the partial gradient with respect to the vector  $y$ :

$$\begin{aligned} \frac{\partial \log L}{\partial y_k} &= \sum_{r=1}^R \left[ -\sum_{j,i} \mathbb{1}[k_i = k] p_{ijr} \left( \frac{y - x_{k_j}}{\beta_r^2} \right) \right. \\ &\quad \left. + \xi(y) \gamma_r \sum_i \sum_{x \in X} \mathbb{1}[k_i = k] (2\pi \beta_r^2)^{-m/2} \left( \frac{y - x}{\beta_r^2} \right) \exp \left\{ -\frac{\|x - y\|^2}{2\beta_r^2} \right\} \right] \quad (15) \end{aligned}$$

This behemoth is difficult to solve analytically. Recall, however, our prior simplifying assumption that  $\forall y, r \sum_{x \in X} g_r(x, y) = 1$ , also enforced a posteriori by means of Eq. 8. The latter portion of Eq. 15 contains the form  $\sum_x (x - y) g_r(x, y)$ , equivalent to taking a quantized version of the expectation of a Gaussian variable subtracted by its own mean (see Eq. 2). A viable approximation to a locally optimal  $y$  embedding point stems from neglecting the contribution of the entire second part of Eq. 15, allowing us to garner the following elegant solution:

$$y_k = \frac{\sum_{r=1}^R \sum_{j,i} \mathbb{1}[k_i = k] p_{ijr} x_{k_j}}{\sum_{r=1}^R \sum_{j,i} \mathbb{1}[k_i = k] p_{ijr}}. \quad (16)$$

Evidently each influence point  $y \in Y$  is attracted to the reception points  $\{x \in X\}$  that demonstrate excitatory influence from it. Unfortunately there is no analogue approximation for the reception points themselves that could manifest by a similar sensible trick. We produce the derivation:

$$\frac{\partial \log L}{\partial x_k} = \sum_{r=1}^R \sum_i \left( \frac{x - y_{k_i}}{\beta_r^2} \right) \left[ -\sum_j \mathbb{1}[k_j = k] p_{ijr} + \xi(y_{k_i}) \gamma_r (2\pi \beta_r^2)^{-m/2} \exp \left\{ -\frac{\|x - y_{k_i}\|^2}{2\beta_r^2} \right\} \right] \quad (17)$$

and submit to regular gradient ascent with learning rate  $\varepsilon$ , and specifically the update rule

$$x_k \leftarrow x_k + \varepsilon \cdot N^{-1} \frac{\partial \log L}{\partial x_k} \quad (18)$$

along the *average* log likelihood for a consistent optimization strategy across different batch sizes. We also include the remark that classic  $L_2$ -regularization may suit applications in which the optimization landscape is not well behaved, thereby subjecting the latent space to a Gaussian prior.

To gain intuition on the selection of  $\varepsilon$ , we looked into *entropic impact* as a heuristic. The beautiful findings in [17] allowed us to reason about the following contribution of a change in an embedding point to the differential entropy of a doubly stochastic point process:

$$\frac{\partial^2 H(k, t)}{\partial t \partial x_k} = [\log \lambda(k, t) + 1] \sum_i \frac{\partial h(k, k_i, t - t_i)}{\partial x_k},$$

which admitted a simple rule of thumb to setting the learning rate w.r.t the averaged log likelihood proportional to  $\frac{h}{N}$ , with the constant pertaining to domain idiosyncrasies. Maintaining this ratio ameliorated convergence in §3.1.

**Diffusion Maps (DM).** Random-walk diffusion methods continue to prove effective in laying e.g. auto-encoded variational priors in a manifold embedding [18, 19, 20]. Construed as graph affinities, the influences  $\Phi$  guide a Markovian random walk of which diffusion maps [21, 22, 23] may be approximated via spectral decomposition. We found that asymmetrical diffusion-maps embeddings (in the style of [24]) serve as an adequate initial condition but are not always conducive to stable learning in conjunction with our dynamic kernel basis.

We review briefly the technique’s application here; the curious reader is encouraged to peruse the theory presented in Coifman’s seminal publications [23]. Casting the influence matrix as edge weights in a bipartite graph flowing between *influence (col.)*  $\leftrightarrow$  *reception (row)*, we examine the diffusion process upon it [24]. We first normalize by density to our liking, per our selected value for the parameter  $0 \leq \alpha \leq 1$  according to

$$A = \text{diag} \left( \left\langle \sum_{l=1}^n \varphi(l, k) \right\rangle_{k=1}^n \right)^{-\alpha} \cdot \Phi \cdot \text{diag} \left( \left\langle \sum_{l=1}^n \varphi(k, l) \right\rangle_{k=1}^n \right)^{-\alpha}. \quad (19)$$

Consider the row-stochastic version of  $A$ , named  $B_R$ . Its singular values multiplied by the left (orthonormal) eigenvectors thereof supply manifold embedding coordinates for the reception points, weighted by significance on accord of the singular values. Likewise,  $B_I$  may be constructed as the row-stochastic transformation of  $A^T$  from the same Eq. 19, of which the resultant coordinates grant us the influence points. In each set of coordinates we preserve only those corresponding to the highest  $m$  singular values, except for the largest that by definition is constant.

**Baseline (B).** In our benchmarks we intended to study the comparative benefits of each embedding scheme, as well as motivate the reason for having an embedding at all (besides the gains in interpretability). Did the reduction in degrees of freedom lend its hand to a more generalizable model of the point process? We pitted the techniques FP and DM against the following:

$$h(k, l, \tau) = \varphi(k, l) \mathbb{1}[\tau > 0] \sum_{r=1}^R f_r(\tau), \quad (20)$$

having estimated the matrix entries  $\varphi(\cdot, \cdot)$  directly as above in Eq. 14.

## 2.4 Initialization

We guessed adequate initial conditions for the EM procedure with a fixed empirical protocol. The surmised influence matrix came by summing up correlations between event types according to an asymmetrical exponential kernel on their time separation.

$$\hat{\varphi}(k, l) = \sum_{i,j} \mathbb{1}[k_j = k, k_i = l] \cdot \hat{\delta} e^{-\hat{\delta}(t_j - t_i)} \quad (21)$$

Notice that it remains unscaled.  $\hat{\delta}$  was computed as the naive reciprocal inter-arrival time between event types  $\hat{t} = n(N-1)^{-1} \sum_{i=1}^{N-1} (t_{i+1} - t_i)$ . We justify this construction on basis of Eq. 9, which forms a weighted average over said arrival times to garner an optimal estimate for  $\delta_r^{-1}$ . We feed the result of Eq. 21 into the diffusion-maps algorithm that is invariant to absolute scale by Eq. 19 in order to obtain our initial embeddings  $(\hat{x}, \hat{y}) \in \hat{X} \times \hat{Y}$ .  $\forall r \hat{\beta}_r^2$  is initialized at the mean dyadic squared distance in the embedding;  $\hat{\delta}_r = (r \hat{t})^{-1}$ , variety in which is injected to nudge the kernels towards different dynamics;  $\hat{\gamma}_r = R^{-1}$  and finally  $\forall x, \hat{\mu}(x) = T^{-1} n^{-1} N$ . We strive to minimize careless bias.

## 3 Results

### 3.1 Synthetic experiments

We contrived a number of scenarios with known ground-truth parameters sampled randomly. The underlying models were always spatiotemporal, with a single kernel  $R = 1$  in the response function, and conforming to the prescription described in this paper. Each sampled model was simulated with the thinning algorithm (see e.g. [25] and their supplementary material) in order to generate a

time-series record of specified length  $N$ . Reception and influence points were realized uniformly from a unit square ( $m = 2$ ). True temporal decay rates  $\delta$  were log-normally distributed; spatial bandwidths  $\beta^2$  were granted a Gamma distribution with shape  $\alpha = 1/\sqrt{n}$  and unit scale. Stability [16] was ensured by setting  $\gamma = 1/\sqrt{n}$ , constraining the Frobenius norm  $\|\Phi\|_F = 1$  that upper-bounds the  $L^2$ -induced norm, which itself upper-bounds the spectral radius of the influences  $\rho(\Phi)$ , the real criterion.

In line with Goodhart’s Law [26], different facets of the model apparatus were scrutinized. First, we noticed a tendency for the baseline to reach high in-sample likelihoods, but abysmal out-of-sample likelihoods in the left tail. This dynamic was conveyed through a total least squares [27] slope and centroid, followed by its root mean-square error (RMSE) in the first four outcome columns of Table 1. Did our models recover the chain of causation? We opened up the empirical  $[p_{i,jr}]$  estimates and computed their Hellinger distance [28] from those stipulated by the ground truth.

Settings	Outcomes							
	( $N$ ) Events	( $n$ ) Types	Ratio	Test	Train	Fit	Div.	Emb. Cor.
FP ( $\varepsilon = 0.75$ , Eq. 18)	300	15	1.09	-4.82	-4.36	0.68	0.14	*0.028
DM ( $\alpha = 1$ , Eq. 19)	300	15	1.47	-5.21	-4.52	0.61	0.12	***0.040
B	300	15	1.33	-5.34	-4.42	0.65	0.20	—
FP ( $\varepsilon = 4.5$ )	300	90	2.85	-18.84	-8.05	1.29	0.39	0.002
DM ( $\alpha = 1$ )	300	90	1.56	-10.01	-7.21	0.92	0.16	-0.005
B	300	90	5.13	-21.81	-6.83	1.17	0.77	—
FP ( $\varepsilon = 0.25$ )	900	15	1.03	-5.79	-5.54	0.42	0.12	-0.012
DM ( $\alpha = 1$ )	900	15	1.01	-3.94	-3.78	0.42	0.08	**0.044
B	900	15	1.10	-6.13	-5.71	0.54	0.14	—
FP ( $\varepsilon = 0.5$ )	900	30	1.11	-4.45	-4.14	0.50	0.09	0.011
DM ( $\alpha = 1$ )	900	30	1.09	-7.62	-7.04	0.63	0.11	*0.020
B	900	30	1.06	-6.87	-6.46	0.55	0.30	—
FP ( $\varepsilon = 0.25$ )	1800	30	1.05	-5.12	-4.91	0.43	0.09	<b>-0.015</b>
DM ( $\alpha = 1$ )	1800	30	1.11	-6.56	-6.20	0.51	0.08	*** <b>0.053</b>
B	1800	30	1.07	-6.83	-6.53	0.42	0.22	—

Table 1: Agglomerate metrics collected in twenty simulated trials per synthetic experiment. A line fit by total least squares revealed an approximate test/train ratio. Outcome columns show, respectively, estimated test/train ratio (col. “ratio”), mean test and train log likelihoods (cols. “test” & “train”), RMSE of the fit line (col. “fit”), divergence from ground-truth causalities (col. “div.”), and mean correlation difference between the model and GloVe along with t-test significance markers (col. “emb. cor.”). \*\*\*,  $P \leq 0.01$ , \*\*,  $P \leq 0.05$ , \*,  $P \leq 0.1$ . Bold numerals indicate the sample rejected an Anderson-Darling test [29] for normality with significance  $\leq 0.05$ .

**Comparison to GloVe.** Our technique lives in a dual realm: that of vector embeddings for words and other sequential entities. We fed the ordered sequence of event-type occurrences into a typical GloVe scheme [30] with a forward-looking window of size three, three dimensions, and an asymmetric cooccurrence matrix in an attempt to recover a set of vectors that served as both influence and reception points.

The final column of Table 1 displays a systematic evaluation against GloVe’s embeddings with reference to the ground-truth geometry. Concretely, all pairwise distances in each setting (that of our learned model and the newfound GloVe embeddings) were correlated to those of the ground truth by Kendall’s rank-based nonparametric statistic [31]. The gap between GloVe’s estimated correlation and the model’s under scrutiny, each in  $[-1, 1]$  and where a positive difference means the model correlated more with the ground truth, was collected in each trial and means along with a t-test significance [32] were reported in the last column of Table 1. GloVe is nondeterministic, so we obtained the sample mean of ten embedding correlations per trial—a move that favors GloVe’s results. From the outcomes, it is evident that DM models pick up the spatial coordinates more consistently—probably due to the regularity imposed by their normalized spectral decomposition.

Model (see §2.3)	Best Train $\log L$	Test $\log L$	Half Life (days)	Best Epoch (0–999)
FP ( $\epsilon = 2$ in Eq. 18)	0.50	-1.18	8.02	179
DM ( $\alpha = 1$ in Eq. 19)	0.058	-1.80	19.27	202
B	0.87	-0.17	7.51	999
Salehi et al. [33]	—	-2.06	—	—

Table 2: Characterization of optimal models for the ebola dataset. Test and train log likelihoods are averages over  $N$ . Under  $R = 2$ , half lives were computed numerically.

### 3.2 Real-world experiments

**Ebola.** Disease contagion within any social apparatus tends to emerge as an excitatory point process. In 2019 a finely regularized variational approach to learning multivariate Hawkes processes from (a little more than) a handful of data [33] was demonstrated on a dataset of infection incidences during the ~2014-2015 ebola outbreak [34]. We gave the record precisely the same treatment they did, and obtained significantly higher commensurate likelihoods than their best case. See Table 2.

**Options market.** The intertwined market activity of options with underlying stocks TSLA, AAPL, and IBM during the arbitrary sequential trading days of September 15 & 18, 2017 lead to 24 distinct event types. Roughly 100,000 total trades per day were sampled on 120% and 80% fuzzy moneyness levels—as portrayed in Figure 2—at the expiration dates 01/18/2019 & 04/20/2018 for both puts and calls. The historical data was procured from AlgoSeek with the generosity of Prof. Roger G. Ghanem. The last 45 minutes of trading comprised each day’s test set. See Table 3: the auxiliary accuracy metric is derived from categorical cross-entropy of the predicted event type at the time of an actual occurrence, rendered by the expression

$$\exp\left\{\mathbb{E}_i \log \frac{\lambda(k_i, t_i)}{\sum_j \lambda(k_j, t_i)}\right\}.$$

We visualized three-dimensional embeddings via their two principal components in Figure 3.

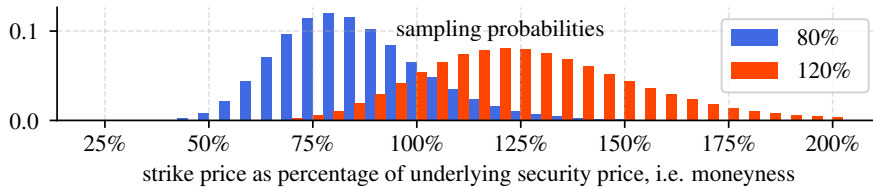


Figure 2: Trades at discrete strike prices were resampled according to quantized log-Gaussian profiles with reference to moneyness at any given point in time. Standard deviations, in logarithmic space, were half the separation between the two densities’ centers.

Dataset	Model	Best Train $\log L$	Test $\log L$	Half Life (min.)	Accuracy
Sep. 15	FP ( $\epsilon = 20$ )	3.05	<b>2.57</b>	$4.09 \times 10^{-4}$	0.119 vs. naive 0.099
	DM	2.85	2.34	$2.26 \times 10^{-4}$	0.103      0.099
	B	2.54	2.11	$1.15 \times 10^{-3}$	0.103      0.099
Sep. 18	FP ( $\epsilon = 1$ )	3.13	<b>2.72</b>	$5.88 \times 10^{-4}$	0.123 vs. naive 0.108
	DM	2.88	2.48	$2.32 \times 10^{-4}$	0.103      0.108
	B	2.75	2.43	$8.78 \times 10^{-4}$	0.117      0.108

Table 3: Market fits with associated half lives. In FP, the best in-sample  $\epsilon$  was picked out of a handful of candidates. Outcome of 200 epochs depicted. Accuracy is obtained from cross entropy.

## 4 Discussion

**Predictive ability.** Our class of models (even “B”) does not struggle with overfitting as much as deep and expressive ones might. Summarily we do not have a validation set, and display the epoch with the best training score in all our experiments. Most notable in Table 1 is how the DM formulation enjoys poorly determined systems, e.g. (300, 90), but is typically outperformed on the basis of likelihoods by FP in better-posed situations like (900, 30). The baseline suffers in recovering actual latent causalities (as depicted by their divergences from ground truth) in contrast to our models.

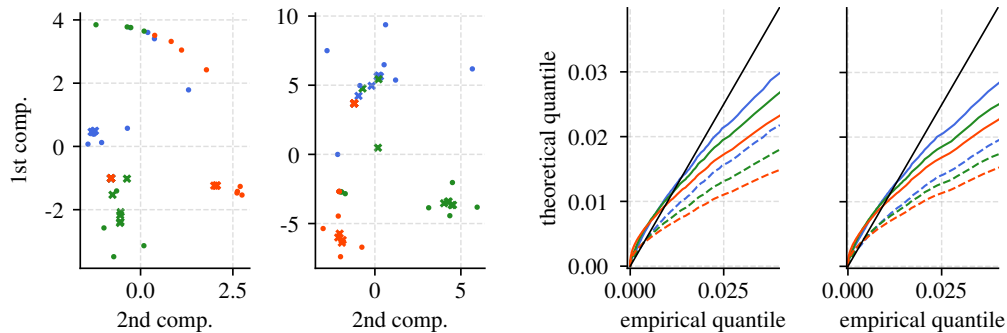


Figure 3: **Left: embeddings** on Sep. 15 and Sep. 18. Eight trade partitions per stock; TSLA is blue, AAPL green, and IBM orange. X’s receive; dots influence. Bandwidths are normalized to one.

**Right: quantile plots**, Sep. 15 & 18, on inter-arrival times of all background (exogenous) market trades versus their supposed Exp. distributions with means that were empirical (solid) and model-derived (dashed), from the sum of all background rates. We depict the cases with no time prior.

**Interpretation of the market embeddings.** Event types of each stock ticker tend to attract influencing points of the same color in Figure 3, with deviations hinting to their relative perceptions by the market. Efficient estimators are necessary in order to discern a lack of stationarity; in this case, transferring our Sep. 15 FP model onto the Sep. 18 test set yielded a  $\log L$  improvement from 2.57 to 2.82, and vice versa gave a decrease from 2.72 to 2.45. Thus behavior largely persists.

The quantile plots put forth that both FP and DM outperformed the baseline in statistically filtering out the white (i.e. serially independent) background events according to their estimated probabilities  $p_{bj}$ . A constant-intensity Poisson process would witness arrival times distributed exponentially [16].

**Disentangling time scales.** We unsuccessfully attempted to sway the estimators towards longer-term (on the order of seconds) behaviors by enlisting a prior on the exponential rate encouraging an expected half life of one minute. Parsing out minute-scale behaviors out of high-frequency trades is severely difficult—recall that most market makers dealing in options are automated. The Gamma prior inflicts a cost without influencing the half lives very much. It would be imperative to study higher-order interactions [35] if one were to investigate longer patterns through individual trades.

## 5 Related Work

We would like to direct the attention of the reader to the meteoric rise of work in Bayesian inference that now permeates serially dependent point processes. Zhang et al. [11] employed Bayesian formulation that samples the branching structure  $p_{ij}$  (see Eq. 7) in order to estimate a particular Mercer expansion of the underlying Gaussian process that constitutes the influence function. Gaussian processes are a prevailing assumption for the direct modulation of the intensity function itself [36, 37, 38, 39, 40]. Linderman and Adams [41] took an approach that estimated a matrix very similar to our  $[\varphi_{ijr}]$ , though relied on discretized binning and variational approximation—both of which we avoid. Salehi et al. [33] exploited a reparametrization trick akin to those in variational autoencoders in order to efficiently estimate the tensor of basis-function coefficients. Apostolopoulou et al. [42] augmented the excitatory model with a nonlinear term that enabled the full a posteriori inference of a model with inhibitions, sans variational approximation. A refreshing perspective on each pairwise interaction as its own process can be found in [43].

Recent progress has been made in factorizing the interaction space with a direct focus on scalability [44]. Additionally, there exist ventures in matching statistics of a Hawkes process with the observed record [16, 45, 46]. Notably Neural Hawkes [25] and a hodgepodge of other techniques centered around neural networks [47, 48, 49, 50, 51, 2, 12, 52, 53] have been established through the years. Our baseline estimator resembles most closely the one described in the work of Zhou et al. [54], whereas the spatiotemporal aspect is inspired from the likes of Schoenberg et al. [13, 3, 14].

## 6 Conclusions

We demonstrated the viability of estimating embeddings for events optimized entirely on the point process dynamics. Our expectation-maximization algorithm extracts the serial dependencies without resorting to variational approximation or a black-box technique.

## References

- [1] G. J. Gibson, G. Streftaris, and D. Thong, “Comparison and assessment of epidemic models,” *Statistical Science*, vol. 33, no. 1, pp. 19–33, 2018.
- [2] X. He, T. Rekatsinas, J. Foulds, L. Getoor, and Y. Liu, “Hawkestopic: A joint model for network inference and topic modeling from text-based cascades,” *International Conference on Machine Learning*, vol. 32, no. 37, pp. 871–880, 2015.
- [3] G. Mohler, “Marked point process hotspot maps for homicide and gun crime prediction in chicago,” *International Journal of Forecasting*, vol. 30, pp. 491–497, 2014.
- [4] G. O. Mohler, M. B. Short, P. J. Brantingham, F. P. Schoenberg, and G. E. Tita, “Self-exciting point process modeling of crime,” *Journal of the American Statistical Association*, vol. 106, no. 493, pp. 100–108, 2011.
- [5] J. W. Pillow, J. Shlens, L. Paninski, A. Sher, A. M. Litke, E. J. Chichilnisky, and E. P. Simoncelli, “Spatio-temporal correlations and visual signaling in a complete neuronal population,” *Nature*, vol. 454, pp. 995–999, 2008.
- [6] M. Morariu-Patrichi and M. S. Pakkanen, “State-dependent hawkes processes and their application to limit order book modeling,” *arXiv:1809.08060v2*, 2018.
- [7] A. Swishchuk and A. Huffman, “General compound hawkes processes in limit order books,” *Risks*, vol. 8, no. 28, 2020.
- [8] K. Drakopoulos, A. Ozdaglar, and J. N. Tsitsiklis, “When is a network epidemic hard to eliminate?,” *Mathematics of Operations Research*, vol. 42, no. 1, pp. 1–14, 2017.
- [9] D. R. Cox, “Some statistical methods connected with series of events,” *Journal of the Royal Statistical Society B*, vol. 17, no. 2, pp. 129–164, 1955.
- [10] A. G. Hawkes, “Spectra of some self-exciting and mutually exciting point processes,” *Biometrika*, vol. 58, no. 1, pp. 83–90, 1971.
- [11] R. Zhang, C. Walder, M.-A. Rizoïu, and L. Xie, “Efficient non-parametric bayesian hawkes processes,” *International Joint Conference on Artificial Intelligence*, vol. 28, 2019.
- [12] N. Du, H. Dai, R. Trivedi, U. Upadhyay, M. Gomez-Rodriguez, and L. Song, “Recurrent marked temporal point processes: Embedding event history to vector,” *KDD*, 2016.
- [13] A. Veen and F. P. Schoenberg, “Estimation of space-time branching process models in seismology using an em-type algorithm,” *Journal of the American Statistical Association*, vol. 103, no. 482, pp. 614–624, 2008.
- [14] B. Yuan, H. Li, A. L. Bertozzi, P. J. Brantingham, and M. A. Porter, “Multivariate spatiotemporal hawkes processes and network reconstruction,” *SIAM J. Math. Data Sci.*, vol. 1, no. 2, pp. 356–382, 2019.
- [15] P. F. Halpin and P. D. Boeck, “Modelling dyadic interaction with hawkes processes,” *Psychometrika*, vol. 78, pp. 793–814, October 2013.
- [16] E. Bacry and J. F. Muzy, “First- and second-order statistics characterization of hawkes processes and non-parametric estimation,” *IEEE Transactions on Information Theory*, vol. 62, no. 4, pp. 2184–2202, 2016.
- [17] J. A. McFadden, “The entropy of a point process,” *Society for Industrial and Applied Mathematics*, vol. 13, no. 4, pp. 988–994, 1965.
- [18] D. Kalatzis, D. Eklund, G. Arvanitidis, and S. Hauberg, “Variational autoencoders with riemannian brownian motion priors,” *arXiv:2002.05227*, 2020.

- [19] H. Li, O. Lindenbaum, X. Cheng, and A. Cloninger, “Diffusion variational autoencoders,” *arXiv:1905.12724*, 2019.
- [20] L. A. P. Rey, V. Menkovski, and J. W. Portegies, “Diffusion variational autoencoders,” *arXiv:1901.08991*, 2019.
- [21] C. Soize and R. Ghanem, “Data-driven probability concentration and sampling on manifold,” *Journal of Computational Physics*, vol. 321, pp. 242–258, 2016.
- [22] W. Lian, R. Talmon, H. Zaveri, L. Carin, and R. Coifman, “Multivariate time-series analysis and diffusion maps,” *Signal Processing*, vol. 116, pp. 13–28, 2015.
- [23] R. R. Coifman and S. Lafon, “Diffusion maps,” *Applied and Computational Harmonic Analysis*, vol. 21, pp. 5–30, 2006.
- [24] K. Pham and G. Chen, “Large-scale spectral clustering using diffusion coordinates on landmark-based bipartite graphs,” *Workshop on Graph-Based Methods for Natural Language Processing*, vol. 12, pp. 28–37, 2018.
- [25] H. Mei and J. Eisner, “The neural hawkes process: A neurally self-modulating multivariate point process,” *31st Conference on Neural Information Processing Systems*, 2017.
- [26] C. Goodhart, *Inflation, Depression, and Economic Policy in the West*, ch. Problems of Monetary Management: The U.K. Experience, pp. 111–146. Rowman & Littlefield, 1981.
- [27] P. de Groen, “An introduction to total least squares,” *arXiv:math/9805076v1*, 1998.
- [28] T. Campbell and X. Li, “Universal boosting variational inference,” *33rd Conference on Neural Information Processing Systems*, 2019.
- [29] N. M. Razali and Y. B. Wah, “Power comparisons of shapiro-wilk, kolmogorov-smirnov, lilliefors and anderson-darling tests,” *Journal of Statistical Modeling and Analytics*, vol. 2, no. 1, pp. 21–33, 2011.
- [30] J. Pennington, R. Socher, and C. D. Manning, “Glove: Global vectors for word representation,” *Conference on Empirical Methods in Natural Language Processing*, 2014.
- [31] R. Newson, “Parameters behind “nonparametric” statistics: Kendall’s tau, somers’ d and median differences,” *The State Journal*, vol. 2, no. 1, pp. 45–64, 2002.
- [32] Student, “The probable error of a mean,” *Biometrika*, vol. 6, no. 1, 1908.
- [33] F. Salehi, W. Trouleau, M. Grossglauser, and P. Thiran, “Learning hawkes processes from a handful of events,” *33rd Conference on Neural Information Processing Systems*, 2019.
- [34] T. Garske, A. Cori, A. Ariyaratnam, I. M. Blake, I. Dorigatti, T. Eckmanns, C. Fraser, W. Hinsley, T. Jombart, H. L. Mills, G. Nedjati-Gilani, E. Newton, P. Nouvellet, D. Perkins, S. Riley, D. Schumacher, A. Shah, M. D. V. Kerkhove, C. Dye, N. M. Ferguson, and C. A. Donnelly, “Heterogeneities in the case fatality ratio in the west african ebola outbreak 2013-2016,” *Philosophical Transactions of the Royal Society B: Biological Sciences*, vol. 372, no. 1721, 2017.
- [35] V. Z. Marmarelis and T. W. Berger, “General methodology for nonlinear modeling of neural systems with poisson point-process inputs,” *Mathematical Biosciences*, vol. 196, pp. 1–13, 2005.
- [36] S. Liu and M. Hauskrecht, “Nonparametric regressive point processes based on conditional gaussian processes,” *33rd Conference on Neural Information Processing Systems*, 2019.
- [37] C. Lloyd, T. Gunter, M. Osborne, S. Roberts, and T. Nickson, “Latent point process allocation,” *International Conference on Artificial Intelligence and Statistics*, vol. 19, no. 51, pp. 389–397, 2016.

- [38] V. Aglietti, E. V. Bonilla, T. Damoulas, and S. Cripps, “Structured variational inference in continuous cox process models,” *33rd Conference on Neural Information Processing Systems*, 2019.
- [39] H. Ding, M. E. Khan, I. Sato, and M. Sugiyama, “Bayesian nonparametric poisson-process allocation for time-sequence modeling,” *arXiv:1705.07006*, 2018.
- [40] S. Flaxman, M. Chirico, P. Pereira, and C. Loeffler, “Scalable high-resolution forecasting of sparse spatiotemporal events with kernel methods,” *arXiv:1801.02858*, 2019.
- [41] S. W. Linderman and R. P. Adams, “Scalable bayesian inference for excitatory point process networks,” *arXiv:1507.03228*, 2015.
- [42] I. Apostolopoulou, S. Linderman, K. Miller, and A. Dubrawski, “Mutually regressive point processes,” *33rd Conference on Neural Information Processing Systems*, 2019.
- [43] Y.-S. Cho, A. Galstyan, P. J. Brantingham, and G. Tita, “Latent self-exciting point process model for spatial-temporal networks,” *Discrete and Continuous Dynamical Systems Series B*, vol. 19, no. 5, pp. 1335–1354, 2014.
- [44] M. Nickel and M. Le, “Learning multivariate hawkes processes at scale,” *arXiv:2002.12501*, 2020.
- [45] M. Achab, E. Bacry, S. Gaiffas, I. Mastromatteo, and J.-F. Muzy, “Uncovering causality from multivariate hawkes integrated cumulants,” *International Conference on Machine Learning*, vol. 34, 2017.
- [46] J. Etesami, N. Kiyavash, K. Zhang, and K. Singhal, “Learning network of multivariate hawkes processes: A time series approach,” in *Proceedings of the Thirty-Second Conference on Uncertainty in Artificial Intelligence*, 2016.
- [47] G. Loaiza-Ganem, S. M. Perkins, K. E. Schroeder, M. M. Churchland, and J. P. Cunningham, “Deep random splines for point process intensity estimation of neural population data,” *33rd Conference on Neural Information Processing Systems*, 2019.
- [48] M. Okawa, T. Iwata, T. Kurashima, Y. Tanaka, H. Toda, and N. Ueda, “Deep mixture point processes: Spatio-temporal event prediction with rich contextual information,” *KDD*, 2019.
- [49] T. Omi, “Fully neural network based model for general temporal point processes,” *33rd Conference on Neural Information Processing Systems*, 2019.
- [50] A. Sharma, A. Ghosh, and M. Fiterau, “Generative sequential stochastic model for marked point processes,” *ICML Time Series Workshop*, 2019.
- [51] J. Shang and M. Sun, “Geometric hawkes processes with graph convolutional recurrent neural networks,” *Association for the Advancement of Artificial Intelligence*, 2019.
- [52] J. Jia and A. R. Benson, “Neural jump stochastic differential equations,” *33rd Conference on Neural Information Processing Systems*, 2019.
- [53] N. Mehrasa, R. Deng, M. O. Ahmed, B. Chang, J. He, T. Durand, M. Brubaker, and G. Mori, “Point process flows,” *arXiv:1910.08281*, 2019.
- [54] K. Zhou, H. Zha, and L. Song, “Learning triggering kernels for multi-dimensional hawkes processes,” in *Proceedings of the Thirtieth International Conference on Machine Learning*, 2013.